Early spin determination at the LHC?

Gudrid Moortgat-Pick[a,b], Krzysztof Rolbiecki[a,*], Jamie Tattersall[c]

[a] *DESY, Deutsches Elektronen-Synchrotron, Notkestr. 85, D-22607 Hamburg, Germany*
[b] *II. Institut für Theoretische Physik, University of Hamburg, Luruper Chaussee 149, D-22761 Hamburg, Germany*
[c] *Universität Bonn, Physikalisches Institut, Nußallee 12, 53115 Bonn, Germany*

Abstract

If signals of new physics are discovered at the LHC it will be crucial to determine the spin structure of the new model. We discuss a method that can help to address this question with a low integrated luminosity, $\mathcal{L} = 1$ fb^{-1}, at $\sqrt{s} = 14$ TeV. Based on the differences in angular distributions of primarily produced particles we show that a significant difference can be observed in the final state jet-pairs rapidity distance. An additional advantage of the method is that it does not rely on any particular structure of the couplings in the decay chain. We simulate samples for models with supersymmetric and UED-like spin structure and show that a distinction can be made early on.

arXiv:1102.0293v2 [hep-ph] 3 Apr 2011

1. Motivation

The Large Hadron Collider (LHC) has started operating and will soon probe physics at the TeV scale, perhaps revealing the origins and mechanism of the electroweak symmetry breaking. One of the most promising candidates for explaining this phenomenon is supersymmetry (SUSY) [1, 2]. In supersymmetric theories each Standard Model (SM) particle is paired with a superpartner of spin different by 1/2. In particular, spin-1/2 quarks will be accompanied by spin-0 squarks, and spin-1 gluons by spin-1/2 gluinos. Another possibility is provided by models with universal extra dimensions (UED) [3]. In such models each SM particle will have a tower of different mass Kaluza-Klein (KK) partners of the same spin.

Since different models of new physics predict different spins for the newly discovered states, the determination of spins will be of extreme importance for establishing the new theory. Generically, SUSY and UED also have a different mass structure, but model-independent measurements of both masses and spins will be required in order to get handle on the underlying model. In this Letter we consider the possibility of distinguishing models with the same mass structure but the spin structure of either SUSY or UED. We will not refer here to any particular UED model, assuming only that it inherits all the properties (masses and couplings) of the analyzed SUSY scenario apart from the spin. Whilst we are only interested in the generic spin structure, we will refer to the same-spin partners as KK-particles for ease of notation. As a benchmark we choose two mSUGRA derived scenarios.

So far there have been a number of features suggested that would hint at the particular spin structure at the LHC (see also [4]):

- The total cross section [5].
- Observation of higher KK modes [6].
- Kinematic distributions of quarks from quark partners decays [7, 8].
- Particle production in vector boson fusion [9].
- Invariant masses of lepton-jet [10, 11, 12, 13, 14] and lepton-photon [15] pairs in squark/KK-quark and gluino/KK-gluon [16] decay chains.
- Kinematic reconstruction of missing momentum [17, 18].
- Angular distributions of leptons from sleptons [19, 20, 21] or s-channel resonances decays [22], and b-jets from bottom squarks decays [23].

Most of these methods require significant statistics and consequently a high luminosity (typically $\mathcal{L} \sim \mathcal{O}(100)$ fb^{-1}) or a very specific decay chain. Here, we propose an extension of the method originally proposed in [19] for sleptons, to the first and second generation squarks/KK-quarks. In a large class of models, strongly-interacting states will provide the first observation of any new physics. Therefore, they offer the opportunity to get hints of the spin structure with early data. Here, we consider an integrated luminosity of $\mathcal{L} = 1$ fb^{-1} at 14 TeV center-of-mass energy (cms), however, the method is also applicable at lower center-of-mass energies.

The Letter is organized as follows. In the next section we define our observable and present a proof of concept that it might be useful in studying spin structure of the underlying model. In Section 3 we discuss our benchmark

☆DESY 11-017, Bonn-TH-2011-03
*Corresponding author
Email address: krzysztof.rolbiecki@desy.de (Krzysztof Rolbiecki)

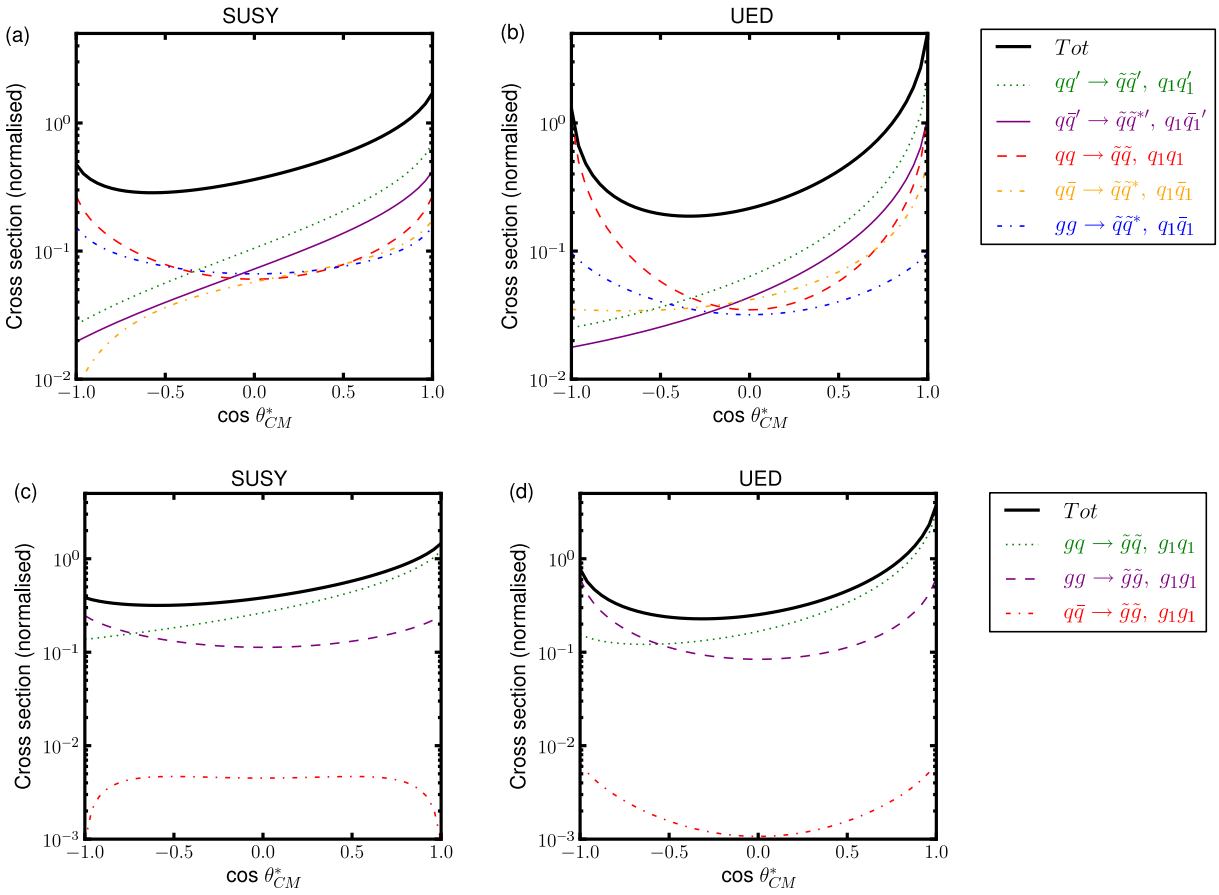

Figure 1: Polar distributions of (a) squarks, (b) KK-quarks, Eq. (1); (c) gluinos, (d) KK-gluons, Eq. (2), in the hard process CM frame normalized to the respective total cross sections at $\sqrt{s} = 14$ TeV. Contributions from left and right states have been summed over. For simplicity we take $m_{\tilde{q}} = m_{\tilde{g}} = 500$ GeV, however, a departure from this assumption does not change the qualitative behaviour of the cross sections. Note that, as dictated by the hard process matrix element, the curves with distinguishable particles in the initial and final state are not symmetric with respect to the incoming parton but will be symmetric with respect to the proton beam.

scenario and details of the event simulation. Section 4 contains the results of the simulations and discussion. Finally, we conclude in Section 5.

2. Spin-sensitive observable

The production of gluinos and squarks of the 1st and 2nd generation is in many scenarios a dominant source of supersymmetric particles. It is, therefore, one of the most promising channels for SUSY searches at the LHC [24]. We will show in this Letter that with early data (1 fb^{-1}) we can already deduce important hints about the spin of the produced particles. We focus here on the di-jet channel (i.e. at least two hard jets, see Sec. 4 for details) for which the sample sources at the parton level are

$$pp \to \tilde{q}_i\,\tilde{q}_j^{(\prime)}\ , \qquad pp \to \tilde{q}_i\,\tilde{q}_j^{*(\prime)}\ , \tag{1}$$

$$pp \to \tilde{g}\,\tilde{g}\ , \qquad pp \to \tilde{g}\,\tilde{q}_i\ , \tag{2}$$

as well as the charge conjugated processes (for squarks), followed by the decays e.g.

$$\tilde{q}_i \to q\,\tilde{\chi}_n^0, \qquad \tilde{q}_i \to q'\tilde{\chi}_k^{\pm}, \qquad \tilde{g} \to q\,\tilde{q}_i, \qquad \text{etc.}, \tag{3}$$

where $i,j = L,R$, $n = 1,\ldots,4$, $k = 1,2$ and q' denotes a quark of different flavour. Of course, the decay chains will very much depend on the details of the spectrum of the model. One particular example leading to a di-jet signal common in mSUGRA scenarios is

$$pp \to \tilde{q}_R\,\tilde{q}_R \to q\,q\,\tilde{\chi}_1^0\,\tilde{\chi}_1^0\ , \tag{4}$$

whereas in UED the respective process is

$$pp \to q_{R1}\,q_{R1} \to q\,q\,\gamma_1\,\gamma_1\ , \tag{5}$$

where q_{R1} and γ_1 are the KK-partners of the right-handed quark and the photon, respectively. However, many different processes from Eqs. (1)+(3) and (2)+(3) can contribute to the di-jet final state and therefore, we consider a fully inclusive signal. In addition, at a hadron collider, extra QCD jets will appear when we include initial state radiation (ISR) and final state radiation (FSR).

Depending on the spin of the primarily produced particle, the distributions in the center-of-mass (CM) frame of the system will be substantially different. Here we focus on the comparison between SUSY models and those with a UED-like spin structure where the quark partners

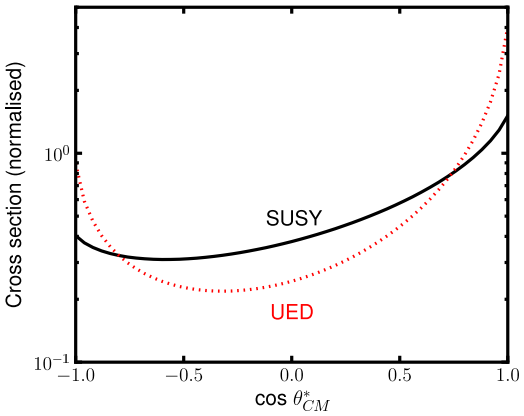

Figure 2: Normalized polar distributions of squarks (black solid) and KK-quarks (red dotted) in the hard process CM frame for $m_{\tilde{q}} = m_{\tilde{g}} = 500$ GeV with cms 14 TeV and with all contributions from strong-interacting states summed over.

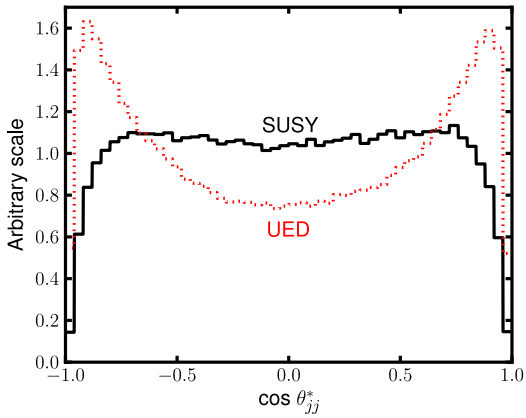

Figure 3: Parton level distribution of $\cos\theta^*_{qq}$, Eq. (6), for SUSY (black solid), Eq. (4), and UED (red dotted), Eq. (5), in the pp CM frame for $m_{\tilde{q}} = m_{\tilde{g}} = 500$ GeV and $m_{\tilde{\chi}^0_1} = 100$ GeV at $\sqrt{s} = 14$ TeV.

are spin-0 and spin-1/2, respectively, whereas the gluon partners carry spin-1/2 and spin-1, respectively. Distributions for the production cross section, process (1) and (2), at the leading order have been calculated in the literature and can be found in e.g. [25, 26, 27, 28, 29, 30] for SUSY and in [11, 31] for UED. Since the shape and relative size of the production channels depends on the collision energy, we fold in the relevant parton density functions (PDFs). This gives an effective polar CM angular distribution with respect to the beam at the LHC in both cases, see Fig. 1. The distributions in Fig. 1 have been calculated at the leading order, but we note that for SUSY, the next-to-leading order (NLO) result is known [30]. The shape of the distributions remain nearly unchanged though and only the total cross sections differ.

Different channels of squark/gluino (KK-quark/KK-gluon) production exhibit a different angular dependence (see e.g. [29]), however when comparing SUSY and UED one clearly sees that the production of supersymmetric particles (spin-0 quarks and spin-1/2 gluinos) tends to be more central compared to KK-particles (spin-1/2 KK-quarks, spin-1 KK-gluons), Fig. 1. The difference between the two spin structures is shown clearly in Fig. 2 by summing over all channels. The main contribution to this effect comes from the fact that, depending on the final states under consideration, SUSY particles will be produced in either an S- or P-wave excitation. Particles produced in a P-wave, due to angular momentum conservation, will have the polar distribution vanishing for $\cos\theta^*_{CM} = \pm 1$. On the other hand, KK-particles will be dominantly produced in S-waves where the distribution has a minimum at $\cos\theta^*_{CM} = 0$, for more details see [32, 33]. This conclusion is independent of the particle masses as the KK-particles are produced in a more forward direction for all channels discussed. In addition, the produced particles will be heavily boosted and hence this will affect any decay products originating from the initial particle.

To probe the production distribution more directly, we propose the following observable, originally suggested for slepton production [19], but adapted here for squarks,

$$\cos\theta^*_{qq} = \tanh\left(\frac{\Delta\eta_{qq}}{2}\right) , \qquad \Delta\eta_{qq} = \eta_{q_1} - \eta_{q_2} , \tag{6}$$

where $\Delta\eta_{qq}$ is the difference of the pseudorapidities between the two final state quarks from squarks or KK-quarks decay chains, e.g. Eq. (4) and (5), Fig. 3. As discussed in [19] this variable is the cosine of the polar angle of quarks with respect to the beam axis in the frame where the pseudorapidities of the quarks are equal and opposite. Being a function of the difference of pseudorapidities, it is longitudinally boost invariant. This observable has proven useful in studying the spin of sleptons [19] and sbottoms [23]. Here we apply a similar approach to the case of the 1st and 2nd generation squarks.

The distribution of the quarks in the laboratory frame is also affected by the decay process. In the case of sparticle decay, the angular distribution of quarks will be flat as we have a decaying scalar,

$$\frac{d\sigma}{d\cos\theta^*_q} \propto 1 , \tag{7}$$

where $\cos\theta^*_q$ is the quark polar angle with respect to the squark momentum, boosted to the squark rest frame. The situation is more complicated for KK-fermions. The distribution will now depend on both the chiral coupling structure and the polarization of the KK-quark. For a polarized fermion we have

$$\frac{d\sigma}{d\cos\theta^*_q} \propto 1 \pm \frac{f_L^2 - f_R^2}{f_L^2 + f_R^2}\cos\theta^*_q , \tag{8}$$

where $f_{L,R}$ are left and right-chiral electroweak couplings, respectively. For $f_L = f_R$ we retain the distribution from Eq. (7) and there is no distinction from a scalar decay. For the other extreme case, $f_L = 0$ or $f_R = 0$, the distribution will have a triangular shape. However, since fermions (KK-quarks in this case) will not be fully polarized, in general

the net distribution of quarks will be $\propto 1 \pm \alpha \cos\theta_q^*$ with $0 < \alpha < 1$. Another issue is that anti-fermions will have an oppositely shaped distribution, cf. $\pm$ sign in Eq. (8).

Even if the KK-quarks have a high degree of polarization, it should be noted that at the LHC, the particles are produced with a significant boost. Therefore the dominant structure of the distributions will be due to the production angle of the initially produced particles. Any angular structure from the decaying particles can only be expected to change the distribution by a small amount *regardless of the coupling structure*. In contrast, the majority of methods so far proposed for spin determination at the LHC rely on a specific electroweak coupling structure in the model (namely $f_L \gg f_R$ or $f_L \ll f_R$) [14]. They would also require correct identification of particles in the specific decay chains.

3. Simulation and benchmark points

In order to realistically assess the observability at the LHC, we perform a hadronic level simulation using `Herwig++ 2.4.2` [34, 35, 36] with `MRST 2004LO` PDFs [37]. Events are then analyzed using `Rivet` [38, 39] and the anti-k_t jet algorithm [40, 41] with $\Delta R = 0.5$. The jets are required to be in the central part of the detector, i.e. $|\eta| < 2.5$.

We include the following SM backgrounds in the analysis: $W^{\pm}$+jets, Z+jets and $t\bar{t}$. Matrix elements are generated using `MadGraph` [42] and hadronized using `Herwig++`. We do not include the QCD[1] and di-boson backgrounds here as these are found to be subdominant [24] for the di-jet signal after the cuts listed in Sec. 4. As benchmark scenarios we choose the ATLAS SU3 and SU6 mSUGRA parameter points [24]. The SU3 scenario features lower masses and is slightly above the current ATLAS and CMS exclusion limits [43, 44], with squark masses of $\mathcal{O}(650)$ GeV. For the slightly heavier SU6 scenario the squark masses are in the range of $\mathcal{O}(850)$ GeV. Masses and parameters for both scenarios are given in Tab. 1. The total NLO SUSY cross sections are 22.9 pb and 6.2 pb for SU3 and SU6, respectively. We simulate the samples of signal and backgrounds corresponding to an integrated luminosity of 1 fb^{-1} at $\sqrt{s} = 14$ TeV for both scenarios. Due to different spins, the total cross section for UED is larger than for SUSY assuming the same masses (by a factor ~ 10 in our scenarios). Therefore, we normalize the number of UED events to the number of SUSY events at NLO calculated using `Prospino` [30] for our comparison.

[1] QCD background is subject to a large theoretical uncertainty $\mathcal{O}(100\%)$. The correct treatment would require full detector simulation, inclusion of higher-order effects and finally the real data. If it turns out that the QCD background is too large, one can use the $2j + \ell$ channel, but this in general would require a higher integrated luminosity [24].

	m_0	$m_{1/2}$	A_0	$\tan\beta$	sign(μ)
SU3	100	300	-300	6	+
SU6	320	375	0	50	+
	$m_{\tilde{g}}$	$m_{\tilde{q}_L}$	$m_{\tilde{q}_R}$	$m_{\tilde{\chi}_1^0}$	$m_{\tilde{\chi}_2^0} \approx m_{\tilde{\chi}_1^\pm}$
SU3	718	670	645	119	222
SU6	885	870	840	152	287

Table 1: mSUGRA parameters and particle masses (in GeV) for SU3 and SU6 scenarios [24]. Masses were calculated using `SPheno 2.3` [45].

4. Numerical results

In our analysis we focus on the 2-jet signal for which we require at least two hard jets but no hard leptons in the final state. In order to suppress the QCD background, relatively high-p_T jets are required along with a hard $E_T^{\rm miss}$ cut. For each of the scenarios we employ the following set of cuts [24]:

- At least two jets with $p_T^{j_1} > 150$ GeV and $p_T^{j_2} > 100$ GeV for the hardest and second-hardest jet, respectively.
- No electrons and muons with $p_T > 20$ GeV and $|\eta_\ell| < 2.5$.
- $\Delta\phi(j_1, E_T^{\rm miss}) > 0.2$, $\Delta\phi(j_2, E_T^{\rm miss}) > 0.2$.
- $E_T^{\rm miss} > 0.3 M_{\rm eff}$.
- $M_{\rm eff} > 800$ GeV,

with the effective mass $M_{\rm eff}$ defined as

$$M_{\rm eff} = p_T^{j_1} + p_T^{j_2} + E_T^{\rm miss} \ .$$

A detailed ATLAS study [24], including a detector simulation, showed that the above mentioned set of cuts give a good signal-to-background ratio ($\sim 2-8$) for SUSY models with $m_{\tilde{q}} \lesssim 900$ GeV and high statistics even at low integrated luminosity ~ 1 fb^{-1}. Therefore, in the present study we focus on the possibility of seeing hints of the spin structure of the new physics at 14 TeV LHC in the early data. However, the same method can be applied at lower center-of-mass energies, albeit with lower statistics.

Our observable, Eq. (6), has to be correspondingly modified at the jet level to be

$$\cos\theta_{jj}^* = \tanh\left(\frac{\Delta\eta_{jj}}{2}\right) \ , \qquad \Delta\eta_{jj} = \eta_{j_1} - \eta_{j_2} \ , \qquad (9)$$

where j_1 and j_2 are the hardest and 2nd hardest jets, respectively. We are analyzing an inclusive SUSY/UED signal, therefore all the channels from Eqs. (1) and (2) will contribute. However, this turns out not to be a problem as

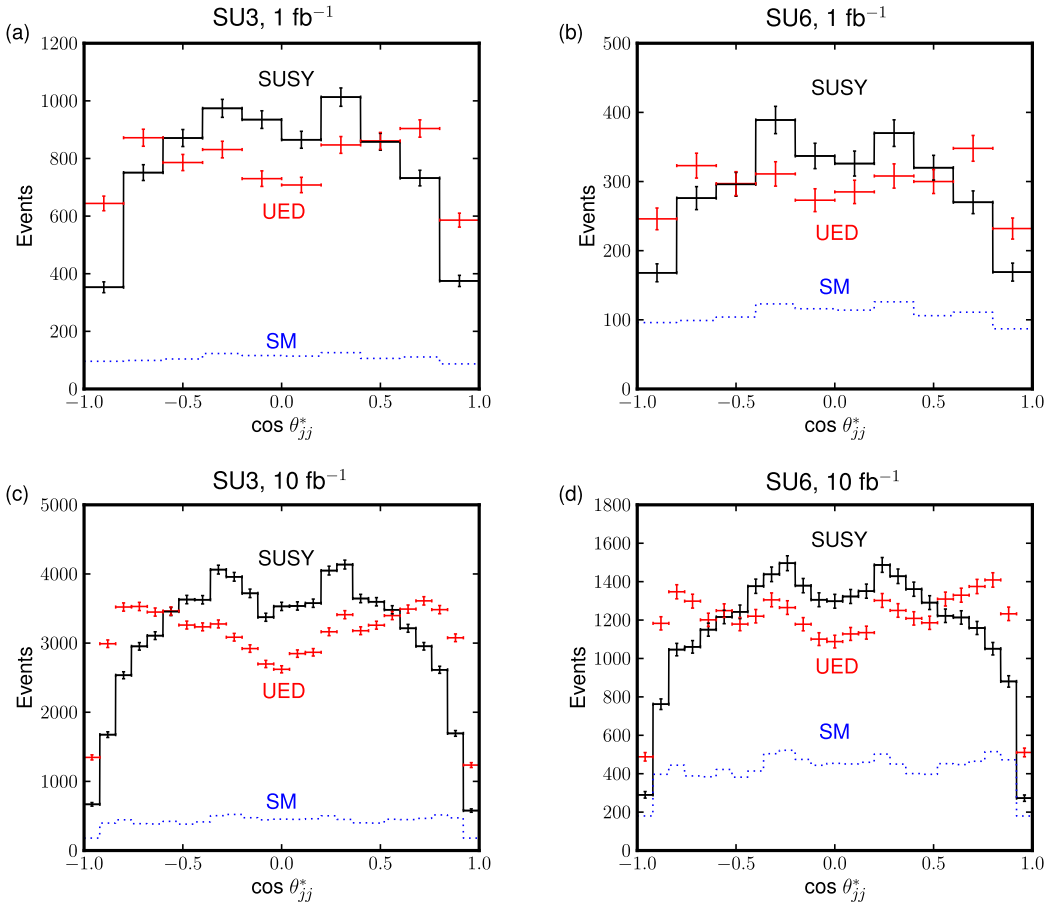

Figure 4: Distribution of pseudorapidity difference for jets, Eq. (9), in SU3 ((a) and (c)) and SU6 ((b) and (d)) scenarios for SUSY (black) and UED (red) spin structure. The dotted blue line is the SM contribution. The number of events corresponds to an integrated luminosity $\mathcal{L} = 1$ fb^{-1} ((a) and (b)) and $\mathcal{L} = 10$ fb^{-1} ((c) and (d)) at 14 TeV cms for SUSY particle production. The number of events for UED has been normalized to the number of SUSY events, respectively. The 1-σ statistical error on each point is shown.

the gluon partners production and the associated quark-gluon partners production all possess the desired features observed for process (4) and (5), see Fig. 1(c) and 1(d).

Note that after the inclusion of hadronization and QCD radiation we are no longer sure whether the observed hard jet originates from a parton from the hard process. This is not a problem in the SUSY-like scenarios discussed here because of the large mass hierarchy, but may be a difficulty in other types of models. For example, if we take the simplest UED model, the mass splitting between the KK-quarks and the KK-photon is normally much smaller than in the models presented here [46]. Consequently, the jets produced when the KK-quarks decay will typically be relatively soft. Isolating these jets will therefore be significantly more difficult and will certainly require a different set of cuts than those used for this study.

Figure 4 shows that even for simulated events, large differences remain between a model with SUSY and UED-like spin structures for both scenarios, left and right panel, respectively. In Fig. 4(a) and 4(b) we expose the clear differences present with 1 fb^{-1} of data. Figures 4(c) and 4(d) show how the situation becomes even clearer after 10 fb^{-1} have been collected. In Fig. 5 we show the limiting case of very high statistics for SUSY and UED, where the qualitative difference between the models is clearly visible.

Several differences can be noted when comparing the hadron-level, Figs. 4 and 5, and the parton-level distributions, Fig. 3. However, these differences can be easily understood once the effect of the experimental cuts have been considered. The first difference is that the number of events where $\cos\theta^*_{jj} \sim \pm 1$ is lower than the parton-level expectation for both SUSY and UED. This is the result of a rapidity cut $|\eta| < 2.5$ on the final state jets. Thus, large rapidity differences between jets are less likely as one or both jets in the observable will not be reconstructed.

We also notice a dip in the distribution centered around $\cos\theta^*_{jj} \sim 0$. The dip is due to the fact that the reconstructed jets have a finite size. Two jets with a small rapidity difference can therefore overlap if they are close in the azimuthal direction and will not be resolved as being separate. Thus, events with this topology will not be reconstructed.

To quantify in one number a clearly visible difference between the distributions we introduce the following asymmetry,

$$\mathcal{A} = \frac{N(|\cos\theta^*_{jj}| > 0.5) - N(|\cos\theta^*_{jj}| < 0.5)}{N_{\rm tot}}\,, \qquad (10)$$

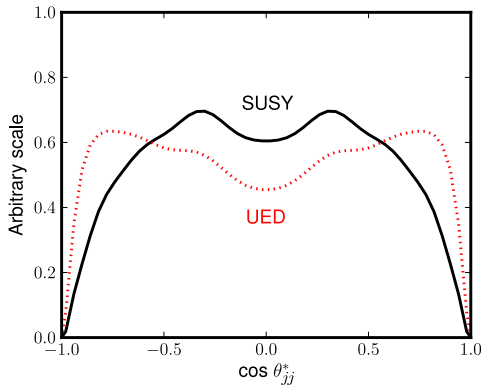

Figure 5: Comparison of distributions between SUSY (solid black) and UED (dotted red) for the limiting case of very high luminosity for the point SU3 at $\sqrt{s} = 14$ TeV.

where $N(\ldots)$ is the number of events fulfilling the respective condition. For our benchmark scenario SU3 at $\mathcal{L} = 1$ fb^{-1} we obtain,

$$\mathcal{A}^{\rm obs}_{\rm SUSY} = -0.22 \pm 0.01\,, \qquad \mathcal{A}^{\rm hl}_{\rm SUSY} = -0.226\,,$$
$$\mathcal{A}^{\rm obs}_{\rm UED} = 0.01 \pm 0.01\,, \qquad \mathcal{A}^{\rm hl}_{\rm UED} = 0.016\,,$$

where $\mathcal{A}^{\rm hl}_{\rm SUSY}$, $\mathcal{A}^{\rm hl}_{\rm UED}$ are the high statistics limits of the asymmetry for SUSY and UED, respectively, and $\mathcal{A}^{\rm obs}_{\rm SUSY}$, $\mathcal{A}^{\rm obs}_{\rm UED}$ are the observed values with statistical errors. Thus, using the outlined method we can clearly distinguish between the two spin structures investigated.

Finally, we consider different possible mass hierarchies of squarks and gluinos (KK-quarks and KK-gluons). The original SU3 and SU6 scenarios feature similar masses of quark and gluon partners, see Tab. 1. Here we also analyze two extreme cases, with either $m_{\tilde{q}} \ll m_{\tilde{g}}$ or $m_{\tilde{q}} \gg m_{\tilde{g}}$. In Tab. 2 we have collected the values of the asymmetry, Eq. (10), for different mass ratios of quark partners to gluon partners. All other parameters are the same as in the SU6 scenario. The values of the asymmetry $\mathcal{A} \approx 0$ and $\mathcal{A} \approx -0.4$ would clearly point to a particular scenario. However, if $\mathcal{A} \approx -0.2$ we are left with an ambiguity, as this value can be obtained in both UED and SUSY scenarios. In principle, the final spin determination would require at least an approximate knowledge of the mass scales in the new physics sector.

Nevertheless, the case with heavy squarks/KK-quarks, $m_{\tilde{q}} \gg m_{\tilde{g}}$, is special since the di-jet signal is produced here by 3-body decays of gluinos/KK-gluons. In particular, neither the cuts nor the observable itself are optimized for this type of the signal. Clearly, in order to come to a decisive conclusion about the spin, an additional observable would have to be included to confirm or exclude 3-body decay case. For example, if gauginos decay to leptons a clear invariant mass, $m_{q\ell}$, edge would point to 2-body quark partner decays. On the other hand, 3-body decays of gluon partners would contain 4 partons in the final state with the similar p_T distributions. In contrast, with quark partners decays, only two high-p_T partons occur in the final state. Therefore, triggering on additional jet activity,

	$m_{\tilde{q}} \ll m_{\tilde{g}}$	$m_{\tilde{q}} \approx m_{\tilde{g}}$	$m_{\tilde{q}} \gg m_{\tilde{g}}$
UED	0.05	0	-0.19
SUSY	-0.22	-0.22	-0.38

Table 2: Comparison of asymmetries, Eq. (10), in SUSY and UED for different mass scenarios of quark and gluon partners. Other parameters are the same as in the SU6 scenario. The statistical error is 0.02, assuming the number of events as in the original SU6 scenario and an integrated luminosity $\mathcal{L} = 1$ fb^{-1}.

together with the study of angular distributions and invariant masses, should in principle allow us to separate these two cases. We also note that heavy quarks/gluon partners would significantly lower the cross sections, hence more integrated luminosity would be required.

5. Conclusions

We have presented a method that may help to expose the spin structure of new physics that may be seen in early LHC data. By comparing the distributions of the di-jet rapidity distance for the models of SUSY and UED spin structure, we found that this observable may provide good supporting evidence to discriminate between them. The method relies only on the spin of initially produced strongly-interacting particles. It does not require any particular electroweak coupling structure and it works for many possible decay chains. Therefore, it can be applied to a wide range of scenarios. The results of the simulation show a clear distinction between models already with $\mathcal{L} = 1$ fb^{-1}. Although we have performed the Monte Carlo simulation for $\sqrt{s} = 14$ TeV the same conclusions hold at lower center-of-mass energies, albeit with lower statistics. While more elaborate studies will be needed in order to fully confirm the spins of all individual particles in a model, early hints of the spin structure will help to direct further measurements.

Acknowledgements

The authors wish to thank Wolfgang Ehrenfeld and Giacomo Polesello for valuable discussions. In addition we would like to thank Frank Siegert and Hendrik Hoeth for their help in the use of `Rivet`. JT was supported by the Helmholtz Alliance HA-101 "Physics at the Terascale". We acknowledge the support of the DFG through the SFB (grant SFB 676/1-2006).

References

[1] H. E. Haber and G. L. Kane, *Phys. Rept.* **117** (1985) 75–263.
[2] H. P. Nilles, *Phys. Rept.* **110** (1984) 1–162.
[3] T. Appelquist, H.-C. Cheng, and B. A. Dobrescu, *Phys. Rev.* **D64** (2001) 035002, `arXiv:hep-ph/0012100`.
[4] L.-T. Wang and I. Yavin, *Int. J. Mod. Phys.* **A23** (2008) 4647–4668, `arXiv:0802.2726 [hep-ph]`.

[5] A. Datta, G. L. Kane, and M. Toharia, arXiv:hep-ph/0510204.
[6] A. Datta, K. Kong, and K. T. Matchev, *Phys. Rev.* **D72** (2005) 096006, arXiv:hep-ph/0509246.
[7] M. M. Nojiri and J. Shu, arXiv:1101.2701 [hep-ph].
[8] G. Hallenbeck, M. Perelstein, C. Spethmann, J. Thom, and J. Vaughan, *Phys. Rev.* **D79** (2009) 075024, arXiv:0812.3135 [hep-ph].
[9] M. R. Buckley and M. J. Ramsey-Musolf, arXiv:1008.5151 [hep-ph].
[10] A. J. Barr, *Phys. Lett.* **B596** (2004) 205–212, arXiv:hep-ph/0405052.
[11] J. M. Smillie and B. R. Webber, *JHEP* **10** (2005) 069, arXiv:hep-ph/0507170.
[12] C. Athanasiou, C. G. Lester, J. M. Smillie, and B. R. Webber, *JHEP* **08** (2006) 055, arXiv:hep-ph/0605286.
[13] L.-T. Wang and I. Yavin, *JHEP* **04** (2007) 032, arXiv:hep-ph/0605296.
[14] M. Burns, K. Kong, K. T. Matchev, and M. Park, *JHEP* **10** (2008) 081, arXiv:0808.2472 [hep-ph].
[15] W. Ehrenfeld, A. Freitas, A. Landwehr, and D. Wyler, *JHEP* **07** (2009) 056, arXiv:0904.1293 [hep-ph].
[16] A. Alves, O. Eboli, and T. Plehn, *Phys. Rev.* **D74** (2006) 095010, arXiv:hep-ph/0605067.
[17] W. S. Cho, K. Choi, Y. G. Kim, and C. B. Park, *Phys. Rev.* **D79** (2009) 031701, arXiv:0810.4853 [hep-ph].
[18] H.-C. Cheng, Z. Han, I.-W. Kim, and L.-T. Wang, *JHEP* **11** (2010) 122, arXiv:1008.0405 [hep-ph].
[19] A. J. Barr, *JHEP* **02** (2006) 042, arXiv:hep-ph/0511115.
[20] D. Horton, arXiv:1006.0148 [hep-ph].
[21] C.-Y. Chen and A. Freitas, *JHEP* **02** (2011) 002, arXiv:1011.5276 [hep-ph].
[22] R. Diener, S. Godfrey, and T. A. W. Martin, *Phys. Rev.* **D80** (2009) 075014, arXiv:0909.2022 [hep-ph].
[23] A. Alves and O. Eboli, *Phys. Rev.* **D75** (2007) 115013, arXiv:0704.0254 [hep-ph].
[24] **ATLAS** Collaboration, G. Aad *et al.*, arXiv:0901.0512 [hep-ex].
[25] G. L. Kane and J. P. Leveille, *Phys. Lett.* **B112** (1982) 227.
[26] P. R. Harrison and C. H. Llewellyn Smith, *Nucl. Phys.* **B213** (1983) 223.
[27] E. Reya and D. P. Roy, *Phys. Rev.* **D32** (1985) 645.
[28] S. Dawson, E. Eichten, and C. Quigg, *Phys. Rev.* **D31** (1985) 1581.
[29] H. Baer and X. Tata, *Phys. Lett.* **B160** (1985) 159.
[30] W. Beenakker, R. Hopker, M. Spira, and P. M. Zerwas, *Nucl. Phys.* **B492** (1997) 51–103, arXiv:hep-ph/9610490.
[31] C. Macesanu, C. D. McMullen, and S. Nandi, *Phys. Rev.* **D66** (2002) 015009, arXiv:hep-ph/0201300.
[32] A. Freitas, D. J. Miller, and P. M. Zerwas, *Eur. Phys. J.* **C21** (2001) 361–368, arXiv:hep-ph/0106198.
[33] S. Y. Choi, K. Hagiwara, H. U. Martyn, K. Mawatari, and P. M. Zerwas, *Eur. Phys. J.* **C51** (2007) 753–774, arXiv:hep-ph/0612301.
[34] M. Bahr *et al.*, arXiv:0803.0883 [hep-ph].
[35] M. Bahr *et al.*, arXiv:0812.0529 [hep-ph].
[36] M. Gigg and P. Richardson, *Eur. Phys. J.* **C51** (2007) 989–1008, arXiv:hep-ph/0703199.
[37] A. D. Martin, W. J. Stirling, R. S. Thorne, and G. Watt, *Phys. Lett.* **B652** (2007) 292–299, arXiv:0706.0459 [hep-ph].
[38] A. Buckley *et al.*, arXiv:1003.0694 [hep-ph].
[39] B. M. Waugh *et al.*, arXiv:hep-ph/0605034.
[40] M. Cacciari and G. P. Salam, *Phys. Lett.* **B641** (2006) 57–61, arXiv:hep-ph/0512210.
[41] M. Cacciari, G. P. Salam, and G. Soyez, *JHEP* **04** (2008) 063, arXiv:0802.1189 [hep-ph].
[42] J. Alwall *et al.*, *JHEP* **09** (2007) 028, arXiv:0706.2334 [hep-ph].
[43] **CMS** Collaboration, V. Khachatryan *et al.*, *Phys. Lett.* **B698** (2011) 196–218, arXiv:1101.1628 [hep-ex].
[44] **ATLAS** Collaboration, G. Aad *et al.*, arXiv:1102.2357 [hep-ex].
[45] W. Porod, *Comput. Phys. Commun.* **153** (2003) 275–315, arXiv:hep-ph/0301101.
[46] H.-C. Cheng, K. T. Matchev, and M. Schmaltz, *Phys. Rev.* **D66** (2002) 036005, arXiv:hep-ph/0204342.